2002

Deriving Analytic BRDFs of Metallic Rough Surfaces

Yinlong Sun

Report Number:
02-006

DERIVING ANALYTIC BRDFs OF METALLIC ROUGH SURFACES

Yinlong Sun

Department of Computer Sciences
Purdue University
West Lafayette, IN 47907

CSD TR #02-006
February 2002

Deriving Analytic BRDFs of Metallic Rough Surfaces

Yinlong Sun
Department of Computer Sciences, Purdue University, W. Lafayette, IN, 47907-1398, USA

Abstract

This report proposes an analytic method to derive BRDFs of metallic rough surfaces based on statistical theory. The surfaces are assumed flat on the microscopic scale, homogeneous and isotropic, and possessing Gaussian height distributions. When only one-bounce reflection is considered, a BRDF is a product of the Fresnel coefficient, *free travel probability* (FTP) which accounts for the surface self-shadowing effect, and a statistical distribution factor of the surface. The analytic form of FTP, which is the percentage of rays leaving a surface without being blocked, is obtained from a rigorous calculation based on surface statistical properties including Gaussian height field and correlation function. The analytic result agrees well to numerical simulation. As a single term, the derived BRDF generates a specular highlight for a smooth surface and appears diffuse when surface roughness increases. Method has also been proposed to implement the derived BRDFs along with RGB-based techniques and resources. These features are demonstrated by images of metallic objects rendered using both measured spectra and color-based data. Further applications and extensions of this work are suggested.

Keywords: local illumination, BRDFs, rough surfaces, metallic materials, statistical method

1 Introduction

In computer graphics, interactions between light and objects (or materials) are represented in terms of local and global illumination. While global illumination handles light transport amongst objects, local illumination addresses light scattering from small surface areas. Because the area considered for local illumination is sufficiently small with respect to the eye or to the typical sizes of interested objects, scattering details in the area can be encapsulated into a function which serves as a building block for global illumination. This strategy has greatly reduced the rendering complexity and accelerated the advancement of computer graphics. Generally, local illumination for surface reflection is described by a bi-directional reflectance distribution function (BRDF), denoted by $\rho(\theta_l, \varphi_l, \theta_v, \varphi_v, \lambda)$, where (θ_l, φ_l) and (θ_v, φ_v) specify the lighting and viewing directions, and λ is the wavelength (Figure 1). Therefore, adequately modeling BRDFs is a fundamental problem in computer graphics.

The basic goals for modeling BRDFs are accuracy and compactness; the first is important for the realism of computer-generated images and the second for rendering capability and convenience. Accuracy shows how well a model agrees to the real data of BRDFs. While measurement is the best way to verify a model, it is also valuable to compare the model to numerical simulation. For the compactness goal, the key issue is to minimize the data size for representing BRDFs. Since BRDFs are multi-dimensional, without a compact representation, a graphics renderer will be subject to a tremendous data burden and thus difficult to handle complex scenes.

Although measurement can provide accurate BRDFs, it has a few drawbacks. First, fully measuring a BRDF needs a large number of sample points and the result has a large data size. Second, such a measurement requires special equipment and considerable labor. Moreover, because physical surfaces are diversified and numerous, it is unfeasible to measure all of them. In contrast, the graphics community has widely adopted the empirical method such as the Phong model [Phong75]. One empirical treatment is the decomposition of the entire local illumination into two separate terms that respectively account for diffuse and specular contributions. The diffuse term is always assumed Lambertian, but the specular term varies and relies on another treatment that attempts to characterize the specular behavior with a simple function controlled by a set of parameters. While this method is compact and intuitive, there is uncertainty in its accuracy. This method is not only inadequate in accuracy as commonly believed, but also difficult to verify by experiment because its parameters do not correspond to measurable physical quantities. The lack of verifiability adds to the concern about the involved arbitrariness in the method, especially when the rendering fidelity is highly desired.

Alternatively, one may derive BRDFs analytically based upon reasonable assumptions. Generally speaking, however, such derivation is very challenging. This is not only because a BRDF is multi-dimensional, but also because the overall behavior of local illumination depends substantially on the surface conditions including roughness, substructure, and optical properties of the involved material. Nevertheless, this method eliminates the drawbacks in the measurement and empirical approaches. This is because a derived BRDF is the same as an empirical model in possessing analytic formalism except that the involved parameters are physically meaningful and measurable. Thus such BRDFs can be conveniently verified by measurement or numerical simulation. Besides, since the analytic derivation is traceable, it is easy to locate the error sources and find effective improvements. There are two major approaches to deriving BRDFs. One is based on the microfacet theory [Torrance67], where a surface is assumed comprised of small flat facets. Thus one-bounce reflection can be expressed as a product of the Fresnel coefficient, shadowing factor, and microfacet distribution [Cook82]. The major weakness lies in the shadowing factor. Although many forms have been developed for it, they are either not derived

rigorously or too complex to use. The other approach starts with Kirchhoff integral [Beckmann63, Kajiya85]. However, this approach works only for reflection and cannot handle surface self-shadowing and multiple scattering. In both approaches, current studies still adopt the empirical treatment that separates the total local illumination into diffuse and specular terms, which leaves some arbitrariness on choosing the weights for the two terms.

This report follows the microfacet theory and derives analytic BRDFs of metallic rough surfaces. The physical surfaces in this report are assumed smooth on the scale of microns, homogeneous and isotropic, and possessing Gaussian height fields. While preserving the key idea of the microfacet theory, this work improves upon previous studies in three ways. First, the shadowing factor is replaced with the free travel probability, which is rigorously derived based on the statistical properties of a surface. The analytic result is quite intuitive and agrees well with numerical simulation. Second, this work removes the rigid separation of local illumination into diffuse and specular terms, and consequently BRDFs for one-bounce reflection have only one term. The rationale behind this is that the Lambertian law addresses the entire scattering from a diffuse surface, where reflection includes one-bounce reflections. If a diffuse term appears in addition to the one-bounce term formed by the Fresnel coefficient, shadowing, and a surface distribution factor, then one-bounce reflections are counted twice. The diffuse term might represent some features of multiple scattering, but there is no clear evidence showing how well it does. Therefore, for a model to be strictly verified, it is more appropriate to leave out the diffuse term in order to maintain the clarity that the BRDFs account solely for one-bounce reflections. As will be illustrated by rendered images, our derived BRDFs as a single term generate a specular highlight for smooth surfaces and appear diffuse when the surface roughness increases. This shows that the one-bounce reflection is indeed involved in both specular and diffuse appearances. Finally, methods are proposed to derive Fresnel coefficients from material colors. This links the BRDF-based rendering to the conventional RGB-based techniques and resources.

Section 2 reviews related previous work. As the key component, Section 3 specifies the model assumptions and derives analytic BRDFs in a step-by-step fashion. Section 4 presents the numerical study and Section 5 discusses properties of the derived BRDFs as well as methods to compute Fresnel coefficients. Section 6 shows the rendered images and Section 7 gives conclusions and future directions.

2 Related Work

Microfacet theory was developed by Torrance and Sparrow [Torrance67] and later used to develop reflection model for graphics application by Cook and Torrance [Cook82]. This approach assumes that a surface consists of many planar, perfectly specular, and isotropic microfacets. Thus specular reflection can be expressed as a product of Fresnel coefficient, a shadowing and masking factor, and the Beckmann's distribution for microfacet slope [Beckmann63]. Later, Oren and Nayar [Oren94] applied a similar idea of surface composition to non-Lambertian surfaces by assuming microfacets as Lambertian. While Fresnel coefficient and Beckmann's distribution are well known, the shadowing and masking factor is difficult to compute. There has been significant research on this problem including both early and recent work. Smith [Smith67], Sancer [Sancer69], and van Ginneken [Ginneken98] did rigorous calculations for Gaussian height fields, but their results are rather complicated. On the other hand, the shadow term by Torrance and Sparrow [Torrance67, Blinn77] was based on a surface formed with V-shaped grooves. Recently, Ashikhmin et al. [Ashikhmin00] proposed an intuitive shadowing term to

accommodate general microfacet distributions. Overall, these forms are either not rigorous enough or too complex to use for graphics application.

Kajiya [Kajiya85] proposed to derive reflection models based on Kirchhoff theory, which computes an electric field through an integral over the space boundary using Green's function. This was followed by a comprehensive model of He et al. [He91], which incorporates other factors including polarization, subsurface scattering, and Gaussian height distribution. Kirchhoff theory is attractive because it has a well-defined physical basis and leads to relatively simple forms of analytical solution. While Helmholtz-Kirchhoff integral, which is the basis of Kirchhoff theory, is rigorously correct, the analytical solution [Beckmann63] involves a number of approximations, which are difficult to quantify [Ogilvy91]. Inherently, the theory cannot address multiple scattering [Ogilvy91, Poulin90] and does not apply to the cases of transmission. In contrast, microfacet theory does not have these limitations.

Alternatively, Poulin and Fournier [Poulin90] derived a reflection model based on parallel cylindrical micro-geometry. Westin [Westin92] adopted a simulation-based method calculate BRDFs of complex surfaces. This approach allows one to simulate light scattering in a ray-tracing procedure at surfaces with various micro-geometries. Arvo [Arvo95] also proposed a technique for computing illumination for non-diffuse surfaces using irradiance tensors. Finally, one can directly measure BRDFs of real samples [Ward92, Marschner00]. But there are technical challenges involved in the measurement, mainly because BRDFs are multi-dimensional. Moreover, errors of measurement need to be considered carefully.

On specifications of rough surfaces, usually the height field is described in terms of its deviation from a smooth reference surface. The shape and location of the reference surface is chosen according to the long-range behavior of the surface. There are essentially two aspects to the nature of a random rough surface: the spread of heights about the reference surface and the variation of these heights along the surface. A variety of methods are available to describe these surface properties, but the most widely used descriptions are surface height probability distributions and surface correlation functions [Ogilvy91]. This means that the surface roughness needs to be specified with not only the root mean square (RMS) of the surface heights, but also the correlation length.

3 Analytic Derivation of BRDFs

3.1 Surface Assumptions and Statistical Characterization

The analytic derivation of BRDFs in this report is based upon the following assumptions:

1. The considered physical surface is smooth on or above the scale of microns, i.e. 10^{-6} m.
2. Light penetration into the material body and volume scattering effect are negligible.
3. The surface is homogenous within ΔA, the area considered for local illumination (Figure 1). This implies that the material properties and statistical parameters are the same across ΔA.
4. The surface is isotropic in ΔA. Specifically, the height deviation and correlation length along any horizontal direction are the same.
5. The surface is a randomly rough height field and its probability density is Gaussian.

In Assumption 1, since the surface is smooth on or above the scale of microns, the size of a smooth area is at least ten times larger than light wavelength. Now consider a thin light ray as a plane wave. According to Huygens's principle, a plane wave will be reflected into the mirror direction and the

reflected wave will remain to be a plane wave if the surface smoothness area is much larger than the wavelength [Hecht98]. This validates that ray reflection on the scale of microns is specular and Fresnel's law applies. When a surface contains significant bumps or valleys whose sizes are comparable to or smaller than wavelength, the picture of specular reflection is not valid and a wave-based method has to be used. Such examples include porous materials (work and wood) and fabricated objects (CD ROM surfaces). Also, if a surface is smooth on or above the scale of microns although it is not comprised of planar facets, Assumption 1 is still satisfied. In this sense, Assumption 1 is more specific than the condition of the microfacet theory, that is, the surface is assumed comprised of flat microfacets [Torrance67]. For this reason, we will call a locally smooth area as a *micro-area* instead of microfacet in the following. Normally metallic surfaces satisfy Assumption 1.

Assumption 2 excludes multi-layer surfaces (such as automobile paints and human skins) and transparent or translucent materials (such as marbles and waxes). But metallic surfaces satisfy this assumption well because light penetration into metals is very thin and the volume scattering effect can be safely ignored [Born75]. The rationale here is that we currently only need to focus on the fundamental surface type, as this solution is the basis for modeling the complex cases. On Assumptions 3 and 4, it should be pointed out that the size of ΔA depends on the viewing condition, i.e. the distance D between the surface and the viewpoint. One may choose ΔA such that its subtended angle to the viewpoint is the minimal resolvable angle α_m of the eye, which is about 1 min of arc [Hecht98]. Thus the dimension of ΔA is $\alpha_m D$. Since the eye has the best acuity when an object is located at 25 cm in front of the eye, the minimal resolvable length l_m is about 0.084 mm. Note that even when the size of ΔA is l_m, ΔA still contains many micro-areas that are smooth the scale of microns; this justifies the statistical method for calculating overall light scattering from ΔA. Finally, for Assumption 5, most natural surfaces are rough and their height fields are Gaussian if generated by purely random processes [Thomas99]. Because the surface randomness destroys the phase coherence between reflected rays from different points, light diffraction will not occur. For the same reason, polarization can be ignored.

Since light reflection from ΔA involves many micro-areas, statistical method is valid for the problem. Let us choose the height average (the reference surface) as the $z = 0$ plane, as shown in Figure 2. Then the height probability function for a Gaussian surface has the form of

$$p(h) = \frac{1}{\sqrt{2\pi}\sigma}\exp(-h^2/2\sigma^2), \tag{3.1.1}$$

where h is the surface height and σ is the *standard deviation* or RMS

$$< h^2 >= \int_{-\infty}^{\infty} p(h)h^2 dh = \sigma^2. \tag{3.1.2}$$

In this report we use $< \cdots >$ to denote an average calculation. For convenience of discussion, let

$$g(t) = \frac{1}{\sqrt{2\pi}}\exp(-t^2/2) \tag{3.1.3}$$

be the *standard Gaussian function* and

$$G(t) = \int_{-\infty}^{t} g(t')dt' = \frac{1}{\sqrt{2\pi}}\int_{-\infty}^{t}\exp(-t'^2/2)dt' \tag{3.1.4}$$

the distribution function for $g(t)$. Thus,

$$p(h) = \frac{1}{\sigma}g(h/\sigma) \tag{3.1.5}$$

and the distribution function for the height field is

$$P(z) = \int_{-\infty}^{z} p(h)dh = G(h/\sigma). \tag{3.1.6}$$

It is easy to see that

$$G(+\infty) = 1, \quad P(+\infty) = 1. \tag{3.1.7}$$

Besides, we need *correlation function* or *correlation coefficient*. It is defined by

$$C(\mathbf{r}) \equiv \frac{< h_1(\mathbf{r}_0)h_2(\mathbf{r}_0 + \mathbf{r}) >}{\sigma^2}, \tag{3.1.8}$$

which involves the average of the product of heights at $\mathbf{r}_0$ and $\mathbf{r}_0 + \mathbf{r}$, which are two points on the $z = 0$ plane. Since the surface is homogenous, the correlation function is independent of $\mathbf{r}_0$. Moreover, because the surface is isotropic, we can write $C(\mathbf{r})$ as $C(r)$ where $r = (x^2 + y^2)^{1/2}$. When r is small, correlation is strong and $C(r)$ is close to 1. On the other hand, when r is large, correlation is weak and $C(r)$ approaches 0. Commonly $C(r)$ is described by [Ogilvy91]

$$C(r) = \exp(-r^2/\tau^2), \tag{3.1.9}$$

where τ is the *correlation length*. Thus, a smooth surface has a small σ and large τ while a rough one has large σ and small τ.

3.2 Basic Equations

BRDF is defined as

$$\rho(\theta_l, \varphi_l, \theta_v, \varphi_v, \lambda) \equiv \frac{dL_v(\theta_v, \varphi_v, \lambda)}{L_l(\theta_l, \varphi_l, \lambda)d\Omega_l} = \frac{dL_v(\theta_v, \varphi_v, \lambda)}{L_l(\theta_l, \varphi_l, \lambda)\sin\theta_l d\theta_l d\varphi_l}, \tag{3.2.1}$$

which is the ratio between an infinitesimal radiance dL_v which is reflected into direction (θ_v, φ_v) and an infinitesimal irradiance $L_l d\Omega_l$ which comes in within solid angle $d\Omega_l = \sin\theta_l d\theta_l d\varphi_l$ about direction (θ_l, φ_l) [Bass95]. The reflection geometry and notations are shown in Figure 1. Note that Eq. (3.2.1) does not explicitly contain a cosine function to account for area projection, as such projection has already been included in the radiance and irradiance. If only one-bounce reflections are considered, then dL_v can be expressed as

$$dL_v = L_l(\theta_l, \varphi_l, \lambda)\overline{R}(\delta/2, \lambda)dh'_x dh'_y \int dh p(h, h'_x, h'_y)\Gamma(h, \theta_l)\Gamma(h, \theta_v), \tag{3.2.2}$$

which includes contributions from all possible micro-areas for the given lighting and viewing directions. $\overline{R}(\delta/2, \lambda)$ is the Fresnel coefficient averaged over all polarizations for incident angle $\delta/2$ (Figure 3), and it appears as a prefactor because Fresnel's law applies to the one-bounce reflection. The differential element $dh'_x dh'_y$, where $h'_x = \partial h/\partial x$ and $h'_y = \partial h/\partial y$, specifies the orientation of a micro-area that may contributes dL_v. Function $p(h, h'_x, h'_y)$ is the combined probability for the surface having height h and slopes h'_x and h'_y. Finally, Eq. (3.2.2) integrates over h because a contributing micro-area may have different height.

Function $\Gamma(h, \theta)$ represents the percentage of rays traveling to the infinity without being blocked by the surface among all rays starting from a micro-area with height h and along polar angle θ. As shown in Figure 2, among the rays from the same height and along the same direction, some are free from blocking (such as ray 1) while others are blocked (such as ray 2). Obviously $\Gamma(h, \theta)$ should satisfy

$$0 \le \Gamma(h,\theta) \le 1 \tag{3.2.3}$$

and, because the surface is a height field, a ray leaving along $\mathbf{z}$ will never be blocked, that is,

$$\Gamma(h,\pi/2) = 1. \tag{3.2.4}$$

In Eq. (3.2.2), $\Gamma(h,\theta_l)$ and $\Gamma(h,\theta_v)$ refer to the lighting and viewing directions. Note that $1-\Gamma(h,\theta_l)$ and $1-\Gamma(h,\theta_v)$ correspond to the casting and shadowing factors used in previous studies [Blinn77, Cook82]. In this report we will not make such a distinction and will simply call $\Gamma(h,\theta)$ as the *free travel probability* (FTP) to emphasize its statistical connotation. Since the surface is isotropic, the FTPis independent of the azimuth angle. The analytic form of $\Gamma(h,\theta)$ will be derived based on statistical consideration below.

To write $dh'_x dh'_y$ in terms of angles,

$$dh'_x dh'_y = h' dh' d\varphi = \tan\theta d(\tan\theta) d\varphi = \frac{1}{\cos^3\theta}\sin\theta d\theta d\varphi, \tag{3.2.5}$$

where θ and φ are the polar and azimuth angles for the surface normal $\mathbf{n}$ of a micro-area (Figure 3). Because $\mathbf{n}$ equally subdivides the lighting and viewing directions $\mathbf{l}$ and $\mathbf{v}$,

$$\mathbf{n} = (\mathbf{l}+\mathbf{v})/2\cos(\delta/2), \tag{3.2.6}$$

where δ is the angle between $\mathbf{l}$ and $\mathbf{v}$. Taking the dot product with unit vector $\mathbf{z}$, this gives

$$\cos\theta = \frac{\cos\theta_l + \cos\theta_v}{2\cos(\delta/2)} = \frac{\cos\theta_l + \cos\theta_v}{\sqrt{2+2\cos\delta}}. \tag{3.2.7}$$

Moreover, the value of $\cos\delta$ can be calculated from

$$\cos\delta = \mathbf{l}\cdot\mathbf{v} = \sin\theta_l \sin\theta_v \cos(\varphi_l - \varphi_v) + \cos\theta_l \cos\theta_v. \tag{3.2.8}$$

We will derive BRDF by comparing Eqs. (3.2.1) and (3.2.2). For this purpose, we need to express dL_v in terms of the solid angle $d\Omega_l = \sin\theta_l d\theta_l d\varphi_l$. If we let

$$\sin\theta d\theta d\varphi = J(\theta_l,\varphi_l)\sin\theta_l d\theta_l d\varphi_l, \tag{3.2.9}$$

the problem becomes determining the Jacobian $J(\theta_l,\varphi_l)$ for the transformation from (θ,φ) to (θ_l,φ_l). The relationship has been found to be [Torrance67]

$$\sin\theta d\theta d\varphi = \frac{\sin\theta_l d\theta_l d\varphi_l}{4\cos(\delta/2)}. \tag{3.2.10}$$

Combining Eqs. (3.2.1), (3.2.2), (3.2.5) and (3.2.10), we obtain

$$\rho(\theta_l,\varphi_l,\theta_v,\varphi_v,\lambda) = \frac{\overline{R}(\delta/2,\lambda)}{4\cos^3\theta\cos(\delta/2)} \int dh p(h,h'_x,h'_y)\Gamma(h,\theta_l)\Gamma(h,\theta_v). \tag{3.2.11}$$

Now we are going to calculate the combined probability the free travel probability.

3.3 Combined Probability

For a Gaussian surface, the following holds [Ogilvy91]

$$< h_1(0) h'_{2x}(r) >= \frac{\partial}{\partial x} < h_1(0) h_2(r) >= \sigma^2 \frac{\partial C(r)}{\partial x}. \tag{3.3.1}$$

Using Eq. (3.1.9),

$$\frac{\partial C(r)}{\partial x} = -2xC(r)/\tau^2, \tag{3.3.2}$$

which is 0 for $r = 0$. This leads to

$$< hh'_x >=< h(0)h'_x(0) >= 0. \tag{3.3.3}$$

For the same reason,

$$< hh'_y >= 0. \tag{3.3.4}$$

Eqs. (3.3.3) and (3.3.4) imply that h is uncorrelated with h'_x and h'_y at the same location. Similarly, the correlation between h'_x and h'_y is

$$< h'_{1,x}(0)h'_{2,y}(r) >= \sigma^2 \frac{\partial^2 C(r)}{\partial x \partial y} = \sigma^2 xyC(r)/\tau^4, \tag{3.3.5}$$

which is 0 for $r = 0$. So h'_x and h'_y are also uncorrelated for the same location.

Because h, h'_x and h'_y are uncorrelated to each other, their combined probability can be decomposed into the product of the individual probabilities:

$$p(h, h'_x, h'_y) = p(h)p(h'_x)p(h'_y). \tag{3.3.6}$$

Here $p(h)$ is Gaussian as given by Eq. (3.3.1). Moreover, if a height field is Gaussian, its derivative is Gaussian as well [Beckmann63]. Therefore we can write

$$p(h'_x) = g(h'_x/\sigma'), \quad p(h'_y) = g(h'_y/\sigma'), \tag{3.3.7}$$

where

$$\sigma' = \sqrt{2}\sigma/\tau \tag{3.3.8}$$

is the deviation for the probability distribution of h'_x and h'_y. Thus,

$$p(h'_x)p(h'_y) = \frac{\tau^2}{4\pi\sigma^2}\exp(-\tau^2 h'^2/4\sigma^2) = \frac{\tau^2}{4\pi\sigma^2}\exp(-\tau^2\tan^2\theta/4\sigma^2), \tag{3.3.9}$$

where $h' = \tan\theta$. Substituting Eqs. (3.1.1) and (3.3.9) into (3.3.6), we obtain

$$p(h, h'_x, h'_y) = \frac{\tau^2}{4\pi\sqrt{2\pi}\sigma^3}\exp(-h^2/2\sigma^2 - \tau^2\tan^2\theta/4\sigma^2). \tag{3.3.10}$$

3.4 Free Travel Probability

The key component in this report is the analytic derivation of the free travel probability $\Gamma(h,\theta)$. Consider a ray (such as ray 1 in Figure 2) starting from a surface point with height h_1 and propagating at a slope angle $\gamma = \pi/2 - \theta$. Without losing generality, we choose the coordinates such that the ray lies in the *zx*-plane and the start point of the ray is $x = 0$.

Let $T(x)$ be the probability for the ray to travel over a horizontal distance x without surface blocking. Then the change of $T(x)$ after interval $[x, x+dx]$ can be written as

$$dT(x) = T(x+dx) - T(x) = -kT(x)Q(x)dx, \tag{3.4.1}$$

where k is independent of x and will be determined later, and

$$Q(x) = \text{Prob}(h_2(x) > h_1 + x\tan\gamma) \tag{3.4.2}$$

is the probability for a ray being blocked within interval $[x, x+dx]$ because $h_1 + x\tan\gamma$ is the ray position at x. The consideration for Eq. (3.4.1) is that the change in $T(x)$ should be proportional to the

amount of rays that have already traveled freely over x, the probability of ray blocking in interval $[x, x+dx]$, and the interval length dx.

Since $Q(x)$ is the probability under the condition that the height is h_1 at $x=0$, it should be calculated using the conditional probability $p(h_2 \mid h_1)$ as

$$Q(x) = \int_{h_1 + x\tan\gamma}^{+\infty} p(h_2 \mid h_1) dh_2 \,. \tag{3.4.3}$$

We can calculate $p(h_2 \mid h_1)$ through

$$p(h_2 \mid h_1) = \frac{p(h_2, h_1)}{p(h_1)}, \tag{3.4.4}$$

where $p(h_2, h_1)$ is a *two-point probability*. For a Gaussian surface, given the height deviation σ and correlation coefficient $C(x)$, $p(h_2, h_1)$ is

$$p(h_1, h_2) = \frac{1}{2\pi\sigma^2\sqrt{1-C^2}} \exp\left[-\frac{h_1^{\,2} - 2h_1h_2C + h_2^{\,2}}{2\sigma^2(1-C^2)}\right] \tag{3.4.5}$$

Applying Eqs. (3.3.1) and (3.4.5) to (3.4.4),

$$p(h_1 \mid h_2) = \frac{1}{\sqrt{2\pi}\sigma\sqrt{1-C^2}} \exp\left[-\frac{(h_2 - h_1C)^2}{2\sigma^2(1-C^2)}\right]. \tag{3.4.6}$$

Thus Eq. (3.4.3) becomes

$$Q(x) = \frac{1}{\sqrt{2\pi}\sigma\sqrt{1-C^2}} \int_{h_1 + x\tan\gamma}^{+\infty} \exp\left[-\frac{(h_2 - h_1C)^2}{2\sigma^2(1-C^2)}\right] dh_2 = 1 - G(w(x)), \tag{3.4.7}$$

where G is given in Eq. (3.1.4) and $w(x)$ is defined as

$$w(x) \equiv \frac{h_1(1-C) + x\tan\gamma}{\sigma\sqrt{1-C^2}}, \tag{3.4.8}$$

which is dimensionless.

If we rewrite Eq. (3.4.1) as

$$d\ln T(x) = \frac{dT(x)}{T(x)} = -kQ(x)dx, \tag{3.4.9}$$

the integration over $[0, x]$ yields

$$\ln T(x) - \ln T(0) = -k\int_0^x Q(x)dx \tag{3.4.10}$$

and

$$T(x) = \exp\left[-k\int_0^x Q(x)dx\right] \tag{3.4.11}$$

because $T(0) = 1$. Integrating $Q(x)$ in parts and using Eq. (3.4.7), we have

$$\int_0^x Q(x)dx = x[1 - G(w(x))]\Big|_0^x + \int_{w_0}^{w(x)} xg(w)dw = -x[1 - G(w(x))] + \int_{w_0}^{w(x)} xg(w)dw, \tag{3.4.12}$$

where $dG(t)/dt = g(t)$ is used based on Eq. (3.2.4) and

$$w_0 = w(0) = \frac{\tau \tan\gamma}{\sqrt{2}\sigma} \tag{3.4.13}$$

for $x = 0$ based on Eq. (3.4.8).

It is easy to se that $\Gamma(h_1, \theta)$ is $T(x)$ when $x \to \infty$, that is,

$$\Gamma(h_1, \theta) = T_\infty = T(x)\big|_{x\to\infty}. \tag{3.4.14}$$

According to Eq. (3.4.8), when $x \to \infty$, $w(x) \to \infty$. Thus, Eq. (3.4.12) becomes

$$\int_0^\infty Q(x)dx = \int_{w_0}^\infty xg(w)dw, \tag{3.4.15}$$

because the first term in Eq. (3.4.12) vanishes (note that $1 - G(w)$ approaches 0 faster than $x \to \infty$).

When we consider for the average height $h_1 = 0$. Eq. (3.4.8) becomes

$$w(x) = \frac{x\tan\gamma}{\sigma\sqrt{1-C^2}}. \tag{3.4.16}$$

For large x, $C \to 0$ and

$$w \to \frac{x\tan\gamma}{\sigma}. \tag{3.4.17}$$

Since a ray travels above the reference surface $z = 0$, γ is positive and $\tan\gamma > 0$. Thus for large x,

$$x = \frac{\sigma w}{\tan\gamma}. \tag{3.4.18}$$

We will use this relation to finish the integral in Eq. (3.4.15); this leads to

$$\int_0^\infty Q(x)dx = \frac{\sigma}{\tan\gamma}\int_{w_0}^\infty wg(w)dw = \frac{\sigma}{\sqrt{2\pi}\tan\gamma}\exp(-w_0{}^2/2). \tag{3.4.19}$$

Note that the approximation used here corresponds to replacing the x-w curve with the straight line for $w \geq w_0$, as shown in Figure 4. So we obtain

$$\Gamma_0(\theta) = \Gamma(h = 0, \theta) = \exp\left[-\frac{k\sigma}{\sqrt{2\pi}\tan\gamma}\exp(-w_0{}^2/2)\right]. \tag{3.4.20}$$

Now we need to determine constant k. From Eq. (3.4.20), the exponent should be dimensionless and therefore $k\sigma$ is dimensionless. To qualify for this, $k\sigma$ may take any of σ/τ, σ^2/τ^2, σ^3/τ^3, ... or their inverse forms. However, the FTPshould satisfy the *scaling invariance principle*, that is, $\Gamma(h, \theta)$ remains the same if the value of $\sigma/\tau\tan\gamma$ does not change. The validity of this principle can be easily shown if we rescale the z-axis by a positive constant a. After this rescaling, σ and $\tan\gamma$ become $a\sigma$ and $a\tan\gamma$ respectively, and τ remains unchanged. So $\sigma/\tau\tan\gamma$ is unchanged. On the other hand, this rescaling will not change the situation of ray blocking and $\Gamma(h, \theta)$ because the ray directions and surface heights are rescaled by the same ratio. This shows the invariance of $\Gamma(h, \theta)$ with respect to $\sigma/\tan\gamma$. Similarly, if rescaling the x-axis, we will show that $\Gamma(h, \theta)$ is invariant with respect to $\tau\tan\gamma$. Therefore, $\Gamma(h, \theta)$ is invariant with respect to $\sigma/\tau\tan\gamma$. To satisfy this scaling invariance principle, k must be the form of

$$k = \frac{1}{\tau}. \tag{3.4.21}$$

For convenience of discussion, we define a dimensionless parameter

$$s \equiv \frac{\tau}{\sigma} \tag{3.4.22}$$

and call s as the *surface smoothness parameter*. Obviously, $s > 0$ and a larger s implies a smoother surface. Correspondingly,

$$\Gamma_0(\theta) = \exp\left[-\frac{\tan\theta}{\sqrt{2\pi}s}\exp(-\frac{s^2}{4\tan^2\theta})\right]. \tag{3.4.23}$$

From Eq. (3.4.23), for fixed θ, when $s \to 0$, that is, the surface is very rough, $\Gamma_0(\theta)$ approaches

$$\Gamma_0(\theta) \to \exp\left[-\frac{\tan\theta}{\sqrt{2\pi}s}\right] \to 0. \tag{3.4.24}$$

On the other hand, when $s \to \infty$, that is, the surface is very smooth, $\Gamma_0(\theta)$ approaches

$$\Gamma_0(\theta) = \exp\left[-\frac{\tan\theta}{\sqrt{2\pi}s}\exp(-\frac{s^2}{4\tan^2\theta})\right] \to 1. \tag{3.4.25}$$

These behaviors will be further discussed in Section 4.

3.5 Final Form of BRDFs

From Eqs. (3.2.11) and (3.3.6),

$$\rho(\theta_i,\varphi_i,\theta_v,\varphi_v,\lambda) = \frac{\overline{R}(\delta/2,\lambda)}{4\cos^3\theta\cos(\delta/2)} p(h'_x)p(h'_y) < \Gamma(h,\theta_i)\Gamma(h,\theta_v) > . \tag{3.5.1}$$

A reasonable approximation is to replace the average of $\Gamma(h,\theta_i)\Gamma(h,\theta_v)$ with the values the free travel probabilities for $h = 0$, that is,

$$< \Gamma(h,\theta_i)\Gamma(h,\theta_v) > \simeq \Gamma_0(\theta_i)\Gamma_0(\theta_v). \tag{3.5.2}$$

The rationale here is that $\Gamma(h,\theta)$ is small for negative h and large for positive h, because a ray starting from a valley is more likely to be blocked and from a hill is more likely to be unblocked. Thus, using Eq. (3.3.9), we obtain the final analytic BRDF:

$$\rho(\theta_i,\varphi_i,\theta_v,\varphi_v,\lambda) = \frac{\overline{R}(\delta/2,\lambda)}{16\pi\cos^3\theta\cos(\delta/2)} s^2 \exp(-s^2\tan^2\theta/4)\Gamma_0(\theta_i)\Gamma_0(\theta_v). \tag{3.5.3}$$

The average Fresnel coefficient will be computed in the next section.

4 Numerical Study

Figure 5 plots the curves of $\Gamma_0(\theta)$ given by Eq. (3.4.23) for different smoothness. The values of s are shown near the corresponding curves. For any curve, the value decreases monotonically from 1 to 0 when θ increases from 0 to $\pi/2$. Note that θ here can be the polar angle for either lighting or viewing direction. When s is small (rough surfaces), the values of $\Gamma_0(\theta)$ are significant only for small θ. On the other hand, when s is large (smooth surfaces), $\Gamma_0(\theta)$ is very close to 1 except when θ approaches

$\pi/2$. Figure 5 displays clearly how the curve of $\Gamma_0(\theta)$ changes gradually when s increases from small to large.

Since Eq. (3.4.23) for the derived FTPis the key component in the entire model of BRDFs, we have performed numerical simulation to verify its correctness. First, we need a procedure to generate samples of randomly rough Gaussian surfaces. For this purpose, we adopt the moving average processes [Ogilvy91] which can construct random Gaussian profiles with specified height deviation and correlation length. Figure 6 shows some examples of Gaussian surfaces generated by this method. The top two profiles have the same height deviation and correlation length. The bottom two profiles have smaller height deviations and therefore they are smoother. In the second step of simulation, after a sample profile is generated, a point with $z = 0$ is found on the profile and a ray is created starting from this point at a given polar angle θ. Then a procedure checks if this ray intersects with the profile, i.e. blocked by the surface. Based on the counts of many sample tests, we can estimate the value of $\Gamma_0(\theta)$.

Figure 7 shows the simulated FTPin comparison with the results given by Eq. (3.4.23) for different surface smoothness. The thick curves are from the analytic derivation and the thin waggling curves are from the simulations for the same surface conditions. From left to right the values of surface smoothness for a pair of smooth and waggling curves are 0.1, 0.25, 0.5, 1, 2, and 5, respectively. In this simulation, the total number of samples created for one combination of surface condition and ray angle is 200. This small number is used because the simulation is computationally expensive. If a large number is used, the fluctuation in the simulation curves will be reduced. However, Figure 7 suffices to show good agreement between the analytic expression and numerical simulation.

5 Discussion and Implementation

5.1 BRDF Behavior

It is easy to check that the BRDF in Eq. (3.5.3) satisfies both reciprocity and energy conservation condition. When (θ_i, φ_i) and (θ_v, φ_v) are switched, i.e., switching the lighting and viewing directions, the result in Eq. (3.5.3) remains the same. Moreover, considering $\overline{R}(\delta/2, \lambda) \le 1$ and $\Gamma_0(\theta) \le 1$ and using Eq. (3.2.10),

$$\begin{aligned} &\iint \rho(\theta_i, \varphi_i, \theta_v, \varphi_v, \lambda) \sin\theta_i d\theta_i d\varphi_i \le \frac{s^2}{4\pi} \iint \frac{1}{\cos^3\theta} \exp(-s^2 \tan^2\theta/4) \sin\theta d\theta d\varphi \\ &= \frac{s^2}{4\pi} \iint \exp(-s^2 \tan^2\theta/4) \tan\theta d\tan\theta d\varphi = 1. \end{aligned} \tag{5.1}$$

This shows that the energy conservation condition is satisfied. It should be pointed out that $\overline{R}(\delta/2, \lambda) \le 1$ corresponds to light absorption by the material and $\Gamma_0(\theta) \le 1$ implies multiple scattering effects are not considered.

For very smooth surfaces, $\Gamma_0(\theta) \to 1$, the BRDF's behavior is dominated by

$$\rho(\theta_i, \varphi_i, \theta_v, \varphi_v, \lambda) \propto \exp(-s^2 \tan^2\theta/4). \tag{5.2}$$

This means that the BRDF has significant values (not close to zero) only for very small θ, and the value vanishes very quickly when θ increases. In other words, a strong highlight should occur near $\theta = 0$. At

this condition, **n** (the normal of micro-areas that contribute to the reflection) is parallel with **z**, and therefore $\theta_v = \theta_l$, $\varphi_v = \pi + \varphi_l$ (refer to Figure 3), which is the mirror reflection condition on the macroscopic scale. Also, note that the reflection intensity at the highlight is proportional to s^2.

On the other hand, for very rough surfaces, $s \to 0$, $\exp(-s^2 \tan^2 \theta / 4) \to 1$. So the BRDF's behavior will be dominated by $\Gamma_0(\theta_l)\Gamma_0(\theta_v)$, which is

$$\Gamma_0(\theta_l)\Gamma_0(\theta_v) \to \exp\left[-\frac{\tan\theta_l}{\sqrt{2\pi}s}\right]\exp\left[-\frac{\tan\theta_v}{\sqrt{2\pi}s}\right] \tag{5.3}$$

because s is small. So the BRDF is maximal when $\theta_l = 0$ and $\theta_v = 0$. Since the tangent function is linear in the exponent in Eq. (5.3) as compared to quadratic in (5.2), the intensity of the BRDF is distributed over spatial orientations more widespread. Also, because s appears in the denominator, the rougher a surface is, the more widespread the energy is distributed. But the BRDF does not approach being independent of the viewing angle and therefore it is not Lambertian even for very rough surfaces. However, note that only single-bounce reflection has been considered in deriving Eq. (3.5.3).

5.2 Computing Fresnel Coefficients

With the analytic form of BRDF given by Eq. (3.5.3) and other involved factors studied in Section 3, the remaining term to determine is the average Fresnel coefficient $\overline{R}$. One may measure and represent it using a two-dimensional array. But in practice this is difficult because the measurement requires perfect smoothness of the surfaces. Therefore, it seems more approachable to compute Fresnel coefficients through the spectra of optical constants.

Consider light reflection at a smooth boundary between media 1 and 2. The Fresnel coefficients for parallel and perpendicular polarizations are

$$\begin{cases} R_{\parallel} = \left(\dfrac{n\cos\theta_i - \cos\theta_t}{n\cos\theta_i + \cos\theta_t}\right)^2 \\ R_{\perp} = \left(\dfrac{n\cos\theta_i - \cos\theta_t}{n\cos\theta_i + \cos\theta_t}\right)^2 \end{cases} \tag{5.4}$$

where n is the index of refraction of medium 2 relative to medium 1, and θ_i and θ_t are the incident and refractive angles. The average Fresnel coefficient is

$$\overline{R} = (R_{\parallel} + R_{\perp})/2 \tag{5.5}$$

if we assume that the energy is equally distributed to parallel and perpendicular polarizations. In general, the relative index of refraction is a complex number and depends on wavelength:

$$n(\lambda) = \eta(\lambda) + i\kappa(\lambda), \tag{5.6}$$

where $\eta(\lambda)$ is the *simple index of refraction* and $\kappa(\lambda)$ is the *extinction coefficient*. Both $\eta(\lambda)$ and $\kappa(\lambda)$ are real and together are called *optical constants*. Thus Fresnel coefficients can be calculated analytically through

$$\begin{cases} R_{\parallel} = \dfrac{(\eta^2+\kappa^2)^2\cos^2\theta_i - 2a(\eta^2+\kappa^2)\cos\theta_i + (a^2+b^2)}{(\eta^2+\kappa^2)^2\cos^2\theta_i + 2a(\eta^2+\kappa^2)\cos\theta_i + (a^2+b^2)} \\ R_{\perp} = \dfrac{\cos^2\theta_i - 2a\cos\theta_i + (a^2+b^2)}{\cos^2\theta_i + 2a\cos\theta_i + (a^2+b^2)} \end{cases} \tag{5.7}$$

where

$$\begin{cases} 2a^2 = \sqrt{(\eta^2-\kappa^2-\sin^2\theta)^2 + 4\eta^2\kappa^2} + (\eta^2-\kappa^2-\sin^2\theta)^2 \\ 2b^2 = \sqrt{(\eta^2-\kappa^2-\sin^2\theta)^2 + 4\eta^2\kappa^2} - (\eta^2-\kappa^2-\sin^2\theta)^2 \end{cases}. \tag{5.8}$$

When the data of $\eta(\lambda)$ and $\kappa(\lambda)$ are measured, the average Fresnel coefficient $\overline{R}$ can be obtained using these equations. The spectra of optical constants for common metals are available in literature [Glassner95].

In practical applications, it is possible that the Fresnel coefficients of some material are needed but the optical constants are not measured. In this case, if the spectral reflectance for the normal incidence R_0 is known, the following method is useful to estimate $\eta(\lambda)$ and $\kappa(\lambda)$. From

$$R_0 = \frac{(\eta-1)^2+\kappa^2}{(\eta+1)^2+\kappa^2}, \tag{5.9}$$

we rewrite it as

$$\kappa^2 = \frac{R_0(\eta+1)^2 - (\eta-1)^2}{1-R_0}. \tag{5.10}$$

Considering that $0 < R_0 < 1$, if we let $\eta = 1$, then

$$\kappa = \sqrt{\frac{4R_0}{1-R_0}}. \tag{5.11}$$

Besides this approach, one may also use Schlick's polynomial approximation to obtain the BRDF [Schlick94].

When only color information (such as RGB triplets) is available, we need first to convert a color to a spectral reflectance R_0 of the normal incidence. A number of methods have been proposed to transform colors into spectra. For example, one can perform such transformation by assuming that the reflectance is a linear combination of three basis functions such as Gaussian or Fourier functions [Sun99].

6 Rendering

Figure 8 displays rendered copper plates with different surface smoothness using the derived BRDFs and measured spectra of copper [Glassner95]. In the first row, the BRDFs do not included the two free travel probabilities for the lighting and viewing directions. The second row includes only the FTPfor the viewing direction. The last row includes both free travel probabilities, i.e., using the entire BRDF in Eq. (3.5.3). From left to right the value of smoothness parameter s are 1, 3, 5, 10, and 20, respectively.

Corresponding the reflection varies from diffuse to specular appearance. The highest reflection intensity moves from the center of the plate, above which a point light source is located, to the edge, which corresponds to the mirror reflection highlight location on the plate. In each image of copper plate, the maximum color intensity has been normalized to 255. The reason for doing the intensity is that the true highlight intensities for small s values (rough surfaces) are too low compared to those for large s values (smooth surfaces), because the highlight intensity is proportional to the square of s, as shown in Eq. (3.5.3).

For this viewing condition, the FTP for the viewing direction does not seem to have significant effect on the relative energy distribution over the copper plate, but the FTP for the light direction has strong effect on the left plate, which is roughest. This makes the highlight located at the center of the plate, and the color distribution tends to be more uniform across the plate. This shows that the FTP is very important for rough surfaces while less important for smooth ones.

Figure 9 displays rendered metallic objects with different surface smoothness, using measured data of optical constants [Glassner95]. A point light source is located at the camera position. The three row corresponds correspond to gold, silver, and copper. From left to right the value of smoothness parameter s are 0.5, 0.8, 1, 2, 4, 5, 7, 10, and 20, respectively. Correspondingly, reflection varies from diffuse to specular appearance. Again the maximum intensities have been scaled to 255. The details of color change can be seen from the large silver vase in Figure 10, which has s=1.

Finally, Figure 11 shows vases rendered using the derived BRDFs along with texture mapping. Two point light sources are used, which generate the two vertical highlight strips on the vases. In image (a), the texture works for different surface smoothness while the material is copper. In (b), the texture gives different colors, which can be regarded as metallic paints. The texture colors are first converted into the spectra of the normal incidence then full BRDFs are computed with the derived form of BRDFs, as described in Section 5.2. This shows that a BRDF-based rendering can easily use RGB-based resources.

7 Conclusion and Future Work

This work carries on the microfacet theory and derives analytic BRDFs of metallic rough surfaces. The surfaces are assumed flat on the microscopic scale, homogeneous and isotropic, and possessing Gaussian height distributions. With considering only one-bounce reflections, we express a BRDF as a product of the Fresnel coefficient, FTP, and a statistical factor for surface orientation distribution. The analytic form of FTP, which corresponds to the shadowing term in previous studies, is derived from a rigorous calculation based on the Gaussian height distribution and correlation function of the surface. The derived FTP has a quite intuitive form and it agrees well with numerical simulation. As a single term, the derived BRDF generates a specular highlight for a smooth surface and appears diffuse when the roughness increases. Method has also been proposed to implement the derived BRDFs along with the conventional RGB-based approach and resources. These features and techniques are demonstrated by rendered images of metallic objects using both measured spectra and color-based data.

This work on metallic rough surfaces has several implications. Because most natural surfaces are rough and Gaussian height fields are common, the derived model is widely applicable. Also, metallic surfaces are the simplest case of surfaces because light can hardly penetrate into metals and so volume scattering are negligible. Therefore, modeling such surfaces is a necessary basis for understanding complex surfaces such as multiple layers (human skins and automobile paints) and transparent or translucent

materials (marbles and waxes), because complex surface contain simplex surfaces or interfaces as components. The established framework for deriving BRDFs is possible to be extended to accommodate more general conditions such as inhomogeneous and anisotropic surfaces. Moreover, this works lays the basis for further calculation multiple scattering contributions. It is also possible to relax the assumption on surface smoothness on the scale of microns such that porous materials can be addressed. But this requires one to switch from the ray-based approach to wave-based approach, because scattering by small structures that are comparable to wavelength is sensitive to the wavelength [Born75].

It would be interesting to compare the derived BRDFs in this work to the existing models [Cook82, Ward92, Ashikhmin00]. However, it is difficult to do so because our model involves new surface specification, namely, the surface smoothness defined as the ratio between height deviation and correlation length, and this does not correspond to any parameters in the existing models. Therefore, a comparison between our and an existing model could be misleading, as they cannot be specified for the *same* physical conditions. In fact, the surface correlation length, which is a key parameter in our calculation, was not considered in these previous studies. However, according to the scaling invariance principle proposed near the end of Section 3.4, correlation length is essential for specification of rough surfaces and their reflection model. In this sense, our work is not a simple extension or modification of some previous model. Nevertheless, the FTP in this work corresponds to the shadowing factor used in previous studies. The rigorous derivation from careful assumptions and approximations, the final intuitive analytic form, and good agreement with numerical simulation make the newly derived FTP overstep the previous methods. But overall, the newly derived BRDFs need to be further verified by experimental measurement and numerical simulation. Since the model accounts only for one-bounce reflection, numerical simulation is more effective because a measurement includes multiple-scattering contribution, which is difficult to be separated from one-bounce reflection.

Another extension of this work is to non-Gaussian surfaces, in other words, the height distribution of surface heights need not to be a Gaussian function. Although Gaussian surfaces are common in reality and many studies use this assumption [Beckmann63, Cook82, He92], measurements have shown that many surfaces behave far from Gaussian [Thomas82,Ogilvy91]. The study of surfaces that are produced by various artificial processes, such turned surfaces, revealed that a surface as the result of a single once-off event does not follow well the Gaussian height statistics. Moreover, some surfaces cannot possess Gaussian height distributions because of their inherent asymmetry. For example, surfaces which are gradually worn down by some abrasive process may start with a Gaussian distribution but their distributions will become increasingly skewed towards negative heights [Thomas82]. Handling non-Gaussian surfaces would be very challenging. Many analytic results as well as the calculation methods in this report, such as in Sections 3.3 and 3.4, will no longer hold. However, it should be pointed out that the key equation for deriving FTP, i.e. Eq. (3.4.1), is valid for non-Gaussian surfaces. Also, the scaling invariance principle also holds generally. These components should be useful to establish a generalized framework for studying surfaces with arbitrary height distribution.

8 References

Arvo95 James Arvo, "Applications of Irradiance Tensors to the Simulation of Non-Lambertian Phenomena," *Computer Graphics, Proc. of ACM SIGGRAPH 95*, ACM Press, New York, 1995, pp. 335-342.

Ashikhmin00 Michael Ashikhmin, Simon Premoze, and Peter Shirley, "A Microfacet-based BRDF Generator," Computer Graphics, Proc. of ACM SIGGRAPH 2000, ACM Press, New York, 2000, pp. 65-74.

Bass95 Michael Bass, Eric W. Van Stryland, David R. Williams, William L. Wolfe, *Handbook of Optics*, Volume I & II, McGraw-Hill, New York, 1995.

Beckmann63 P. Beckmann and A. Spizzichino, *The Scattering of Electromagnetic Waves from Rough Surfaces*, Macmillan, New York, 1963.

Blinn77 James F. Blinn, "Models of Light Reflection for Computer Synthesized Pictures," *Computer Graphics, Proc. of ACM SIGGRAPH 77*, Vol. 11, Num. 2, ACM Press, New York, 1977, pp. 192-198.

Born75 Max Born and Emil Wolf, *Principles of Optics: Electromagnetic Theory of Propagation, Interference and Diffraction of Light*, Pergamon Press, Oxford, 1975.

Cook82 Robert L. Cook and Kenneth E. Torrance, "A Reflection Model for Computer Graphics," *ACM TOG*, Vol. 1, No. 1, Jan. 1982, pp. 7-24.

Glassner95 Andrew S. Glassner, *Principles of Digital Image Synthesis*, Morgan Kaufmann, San Francisco, 1995.

He91 Xiao D. He, Kenneth E. Torrance, Francois X. Sillion, and Donald P. Greenberg, "A Comprehensive Physical Model for Light Reflection," *Computer Graphics, Proc. of ACM SIGGRAPH 91*, ACM Press, New York, 1991, pp. 175-186.

Hecht98 Eugene Hecht, *Optics*, Third Edition, Addison-Wesley, Reading, Massachusetts, 1998.

Kajiya85 James T. Kajiya, "Anisotropic Reflection Models," *Computer Graphics, Proc. of ACM SIGGRAPH 85*, Vol. 19, Num. 3, ACM Press, New York, 1985, pp. 15-21.

Marschner98 Steve R. Marschner, *Inverse Rendering for Computer Graphics*, Ph.D thesis, Cornell University, 1998.

Ogilvy91 J. A. Ogilvy, *Theory of Wave Scattering from Random Rough Surfaces*, Adam Hilger, Bristol, 1991.

Oren94 Michael Oren and Shree K. Nayar, "Generalization of Lambert's Reflectance," *Computer Graphics, Proc. of ACM SIGGRAPH 94*, ACM Press, New York, 1994, pp. 239-246.

Phong75 Bui-Tuong Phong, "Illumination for Computer Generated Images," *Communications of the ACM*, Vol. 18, No. 6, 1975, pp. 311-317.

Poulin90 Pierre Poulin and Alain Fournier, "A Model for Anisotropic Reflection," *Computer Graphics, Proc. of ACM SIGGRAPH 90*, Vol. 24, Num. 4, ACM Press, New York, 1990, pp. 273-282.

Sancer69 M. I. Sancer, "Shadow Corrected Electromagnetic Scattering from Randomly Rough Surfaces," *IEEE Transactions on Antennas and Propagation*, Vol. AP-17, No. 5, 1969, pp. 577-585.

Schlick94 C. Schlick, "An Inexpensive BRDF model for Physically-Based Rendering," *Computer Graphics Forum*, Vol. 13, No. 3, 1994, pp. 233-246.

Smith67 Bruce G. Smith, "Geometrical shadowing of a random rough surface," *IEEE Transactions on Antennas and Propagation*, Vol. AP-15, No. 5, 1967, pp. 668-671.

Sun99 Yinlong Sun, F. David Fracchia, Thomas W. Calvert, and Mark S. Drew, "Deriving Spectra from Colors and Rendering Light Interference," *IEEE Computer Graphics and Application*, Vol. 19, No. 4, Jul. 1999, pp. 61-67.

Thomas99 Tom R. Thomas, Rough Surfaces, Second Edition, Imperial College Press, London, 1999.

Torrance67 Kennеth Torrance and E. M. Sparrow, "Theory for Off-specular Reflection from Roughened Surfaces," *J. Opt. Soc. Am.*, Vol. 57, 1967, pp. 1105-1114.

Ginneken98 B. van Ginneken, M. Stavridi, and J. J. Koenderink, "Diffuse and Specular Reflectance from Rough Rurfaces," *Applied Optics*, Vol. *37*, 1 (1998), 130–13.

Ward92 Gregory J. Ward, "Measuring and Modeling Anisotropic Reflection," *Computer Graphics, Proc. of ACM SIGGRAPH 92*, ACM Press, New York, 1992, pp. 265-272.

Westin92 Stephen H. Westin, James R. Arvo, and Kenneth E. Torrance, "Predicting Reflectance Functions from Complex Surfaces," *Computer Graphics, Proc. of ACM SIGGRAPH 92*, ACM Press, New York, 1992, pp. 255-264.

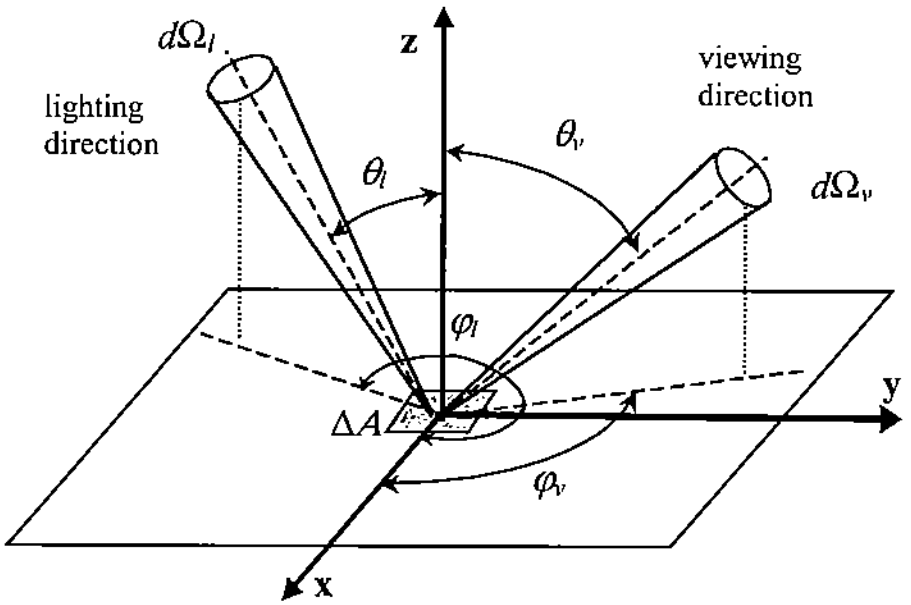

Figure 1: Geometry and notations for light reflection. The small surface area ΔA is considered for computing local illumination.

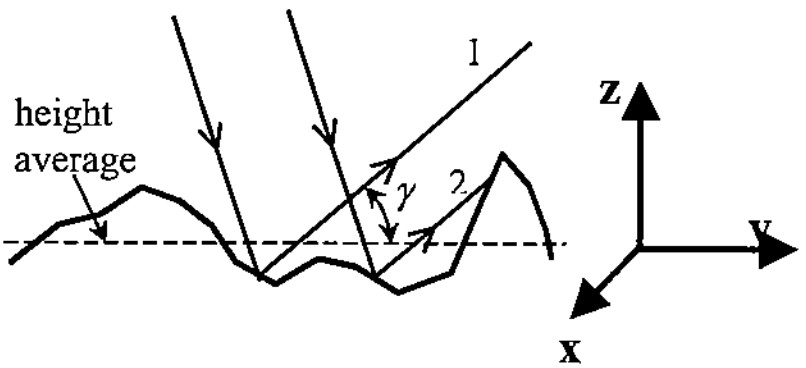

Figure 2: Rough surface profile, ray scattering, and coordinates frame.

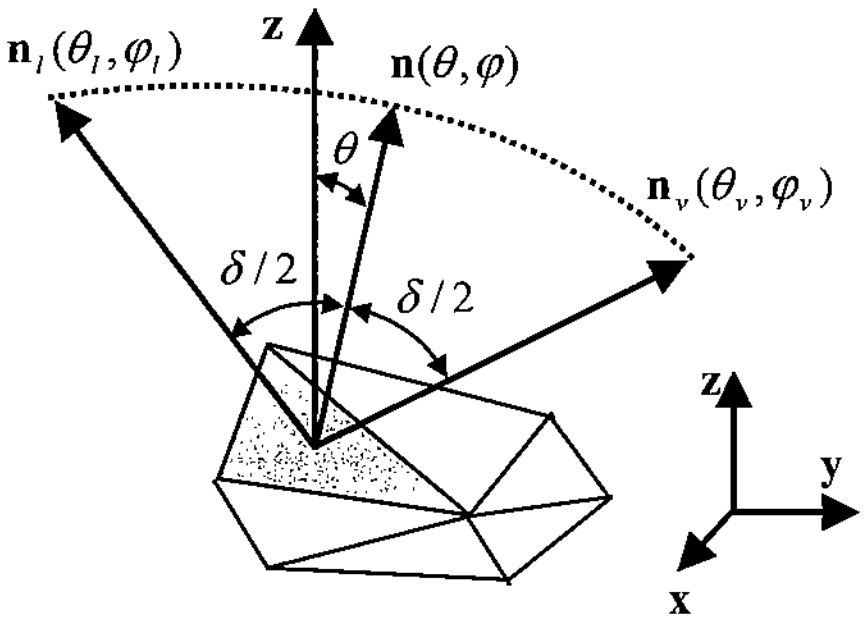

Figure 3: Ray scattering geometry and notations.

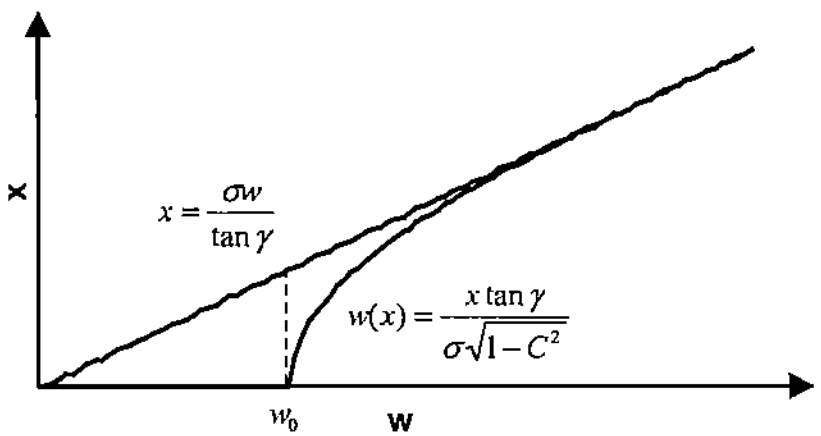

Figure 4: Relations between w and x for fixed γ, σ, and τ. The curve and line are generated using data from numerical calculations.

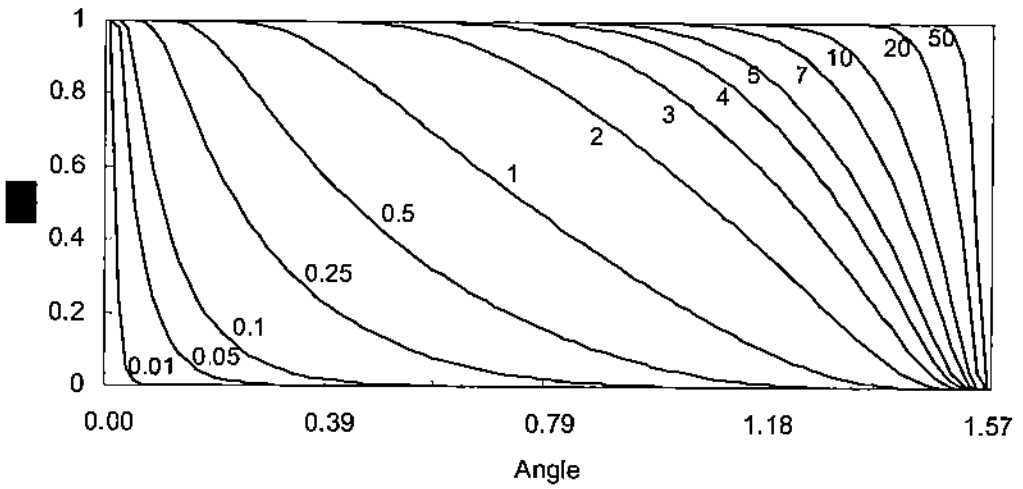

Figure 5: The angular dependency of FTP for different surface smoothness s. The value of s is shown near the corresponding curve.

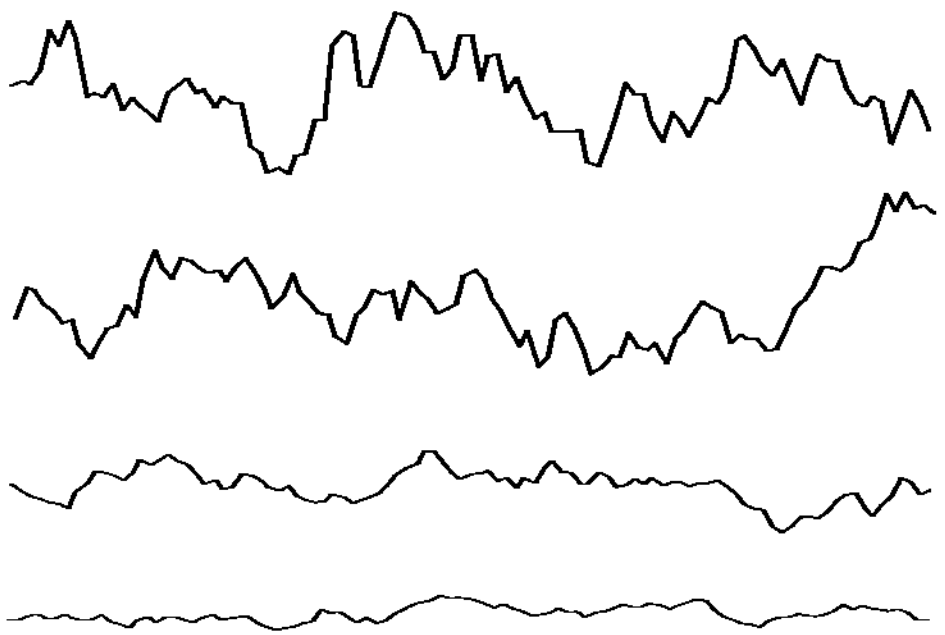

Figure 6: Some profiles of Gaussian surfaces generated by a random procedure for numerical simulation.

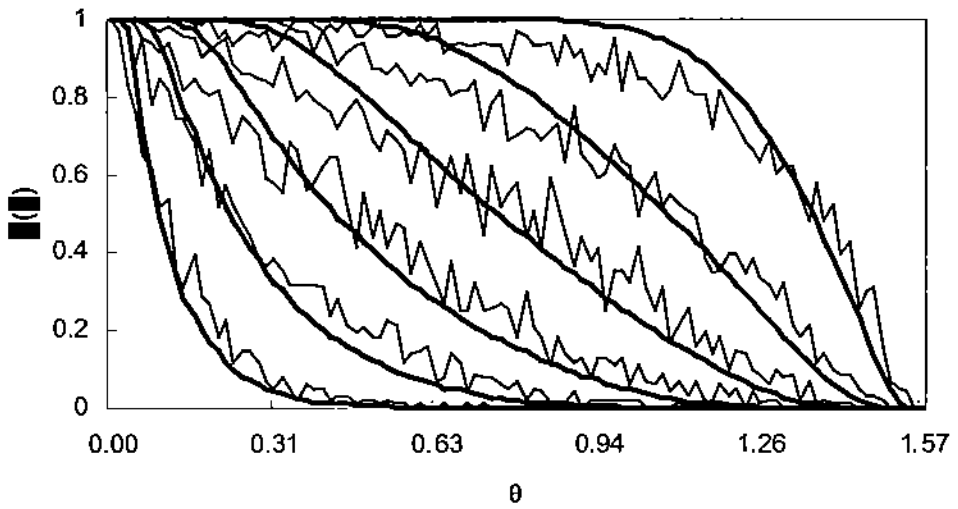

Figure 7: Simulated FTP for a number of surface smoothness values. The thick curves are generated by analytic expression and the corresponding thin waggling curves are by simulation.

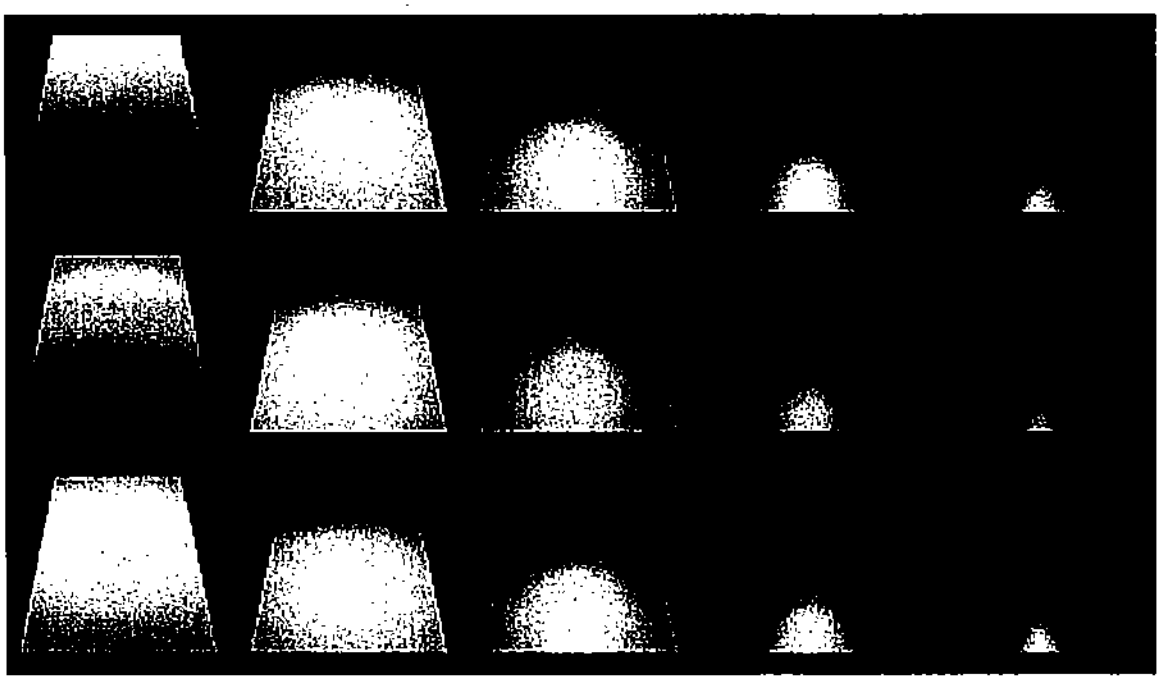

Figure 8: Copper plates rendered the derived analytic BRDF and real copper spectral data. The Images show the effects of the FTP and different surface smoothness.

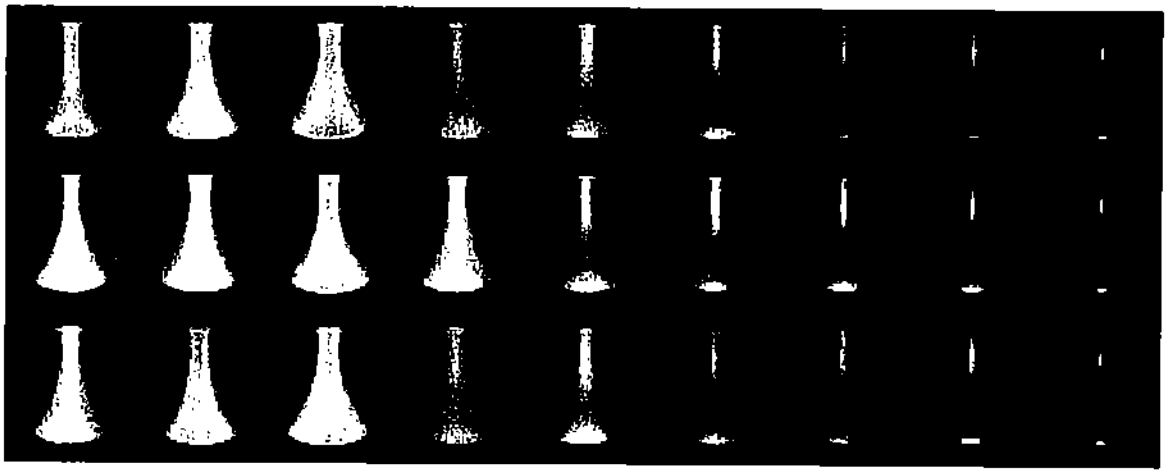

Figure 9: Rendered gold, silver and copper vases for different surface smoothness.

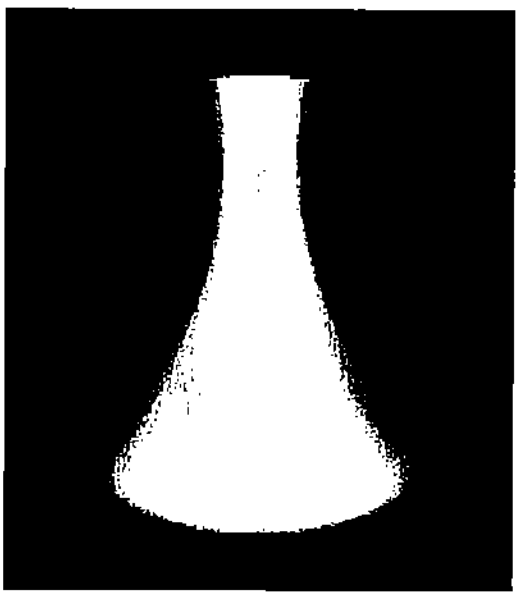

Figure 10: A rendered silver vase with moderate smoothness to show the color change details.

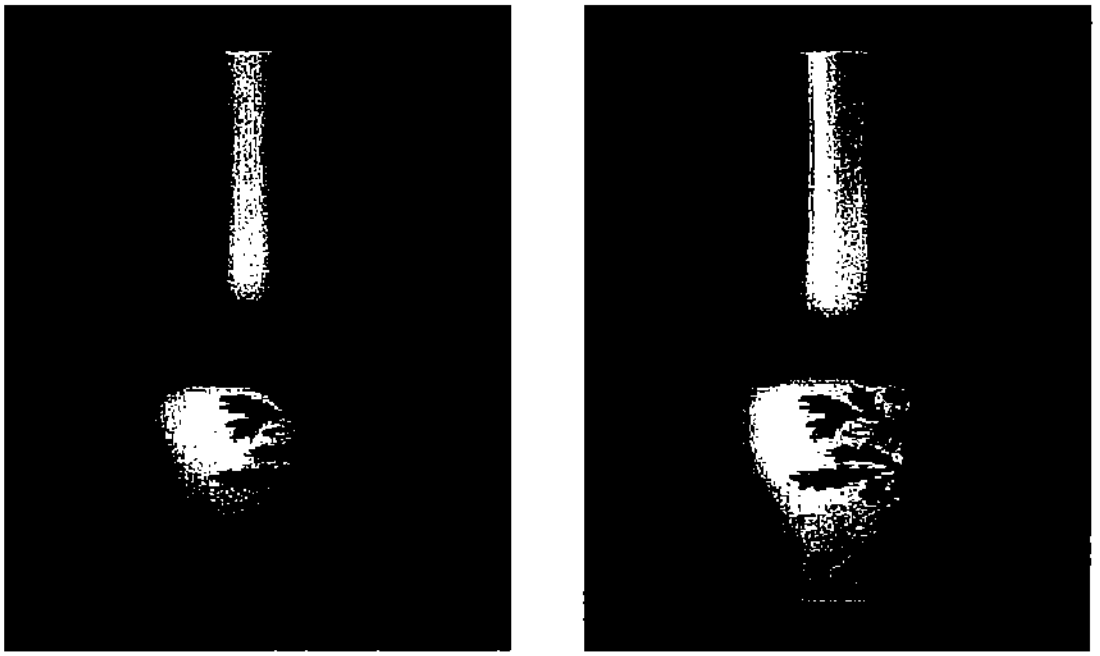

Figure 11: Rendered vases with textures for smoothness (a) and color (b).